Textile piezoelectric sensors – melt spun bi-component poly(vinylidene fluoride) fibres with conductive cores and poly(3,4-ethylene

Downloaded from: https://research.chalmers.se, 2026-10-08 10:03 UTC

Citation for the original published paper (version of record):
Åkerfeldt, M., Nilsson, E., Gillgard, P. et al (2014). Textile piezoelectric sensors – melt spun bi-component poly(vinylidene fluoride) fibres with conductive cores and poly(3,4-ethylene dioxythiophene)-poly(styrene sulfonate) coating as the outer electrode. Fashion and Textiles, 1(1). http://dx.doi.org/10.1186/s40691-014-0013-6

N.B. When citing this work, cite the original published paper.

research.chalmers.se offers the possibility of retrieving research publications produced at Chalmers University of Technology. It covers all kind of research output: articles, dissertations, conference papers, reports etc. since 2004. research.chalmers.se is administrated and maintained by Chalmers Library

(article starts on next page)

Åkerfeldt et al. Fashion and Textiles 2014, 1:13
http://link.springer.com/article/10.1186/s40691-014-0013-6

Fashion and Textiles
a SpringerOpen Journal

RESEARCH Open Access

Textile piezoelectric sensors – melt spun bi-component poly(vinylidene fluoride) fibres with conductive cores and poly(3,4-ethylene dioxythiophene)-poly(styrene sulfonate) coating as the outer electrode

Maria Åkerfeldt[1,2*], Erik Nilsson[1,3], Philip Gillgard[1] and Pernilla Walkenström[1]

* Correspondence:
maria.akerfeldt@swerea.se
[1]Swerea IVFAB, Textiles and Plastics Department, Box 104, SE-43122 Mölndal, Sweden
[2]University of Borås, The Swedish School of Textiles, SE-50190 Borås, Sweden
Full list of author information is available at the end of the article

Abstract

The work presented here addresses the outer electroding of a fully textile piezoelectric strain sensor, consisting of bi-component fibre yarns of β-crystalline poly(vinylidene fluoride) (PVDF) sheath and conductive high density polyethylene (HDPE)/carbon black (CB) core as insertions in a woven textile, with conductive poly(3,4-ethylene dioxythiophene)-poly(styrene sulfonate) (PEDOT:PSS) coatings developed for textile applications. Two coatings, one with a polyurethane binder and one without, were compared for the application and evaluated as electrode material in piezoelectric testing, as well as tested for surface resistivity, tear strength, abrasion resistance and shear flexing. Both coatings served their function as the outer electrodes in the system and no difference in this regard was detected between them. Omission of the binder resulted in a surface resistivity one order of magnitude less, of 12.3 Ω/square, but the surface resistivity of these samples increased more upon abrasion than the samples coated with binder. The tear strength of the textile coated with binder decreased with one third compared to the uncoated substrate, whereas the tear strength of the coated textile without binder increased with the same amount. Surface resistivity measurements and scanning electron microscopy (SEM) images of the samples subjected to shear flexing showed that the coatings without the binder did not withstand this treatment, and that the samples with the binder managed this to a greater extent. In summary, both of the PEDOT:PSS coatings could be used as outer electrodes of the piezoelectric fibres, but inclusion of binder was found necessary for the durability of the coating.

Keywords: Piezoelectric sensor; PVDF; PEDOT:PSS; Textile coating

Introduction

One of the most critical issues to address for the Smart Textiles concept is the integration of the smart components into textile structures (Kirstein 2013). Electroactive components generally lead to perceived bulkiness and loss of flexibility in the textiles. Furthermore, the lack of refined integration methods has been a serious pitfall for the possibilities for industrialization and the following commercialization of products

Springer

© 2014 Åkerfeldt et al.; licensee springer. This is an Open Access article distributed under the terms of the Creative Commons Attribution License (http://creativecommons.org/licenses/by/4.0), which permits unrestricted use, distribution, and reproduction in any medium, provided the original work is properly credited.

deriving from the area. With more sophisticated methods and materials emerging, there is renewed hope of finding solutions that could offer electronics incorporated in the textile materials by industrially feasible methods. Sensing and actuating are vital to many smart textiles applications and have therefore been the focus of much research, but still require more optimal routes to textile integration (Schwarz et al. 2010). To achieve an active sensor, an interesting alternative for textile applications is a polymer that exhibits piezoelectric properties, i.e. generates an electric potential from deformation, such as poly(vinylidene fluoride) (PVDF).

PVDF is polymorphic and has four crystalline phases: α, β, γ and δ. The β-phase crystal structure is the most polar, which is required for piezoelectric properties in a polymeric material (Fukada and Takashita 1969; Kawai 1969). When PVDF solidifies from a melt or a solution, the normal scenario is that it crystallizes to form the non-polar α-phase. The α-phase can be transformed to β-phase crystallinity by mechanical deformation, such as drawing of films (S. H. Lee and Cho 2010). It was recently found that the same effect can be achieved with sufficient cold drawing, i.e. drawing in the temperature interval between T_g and T_m, during the melt spinning process of PVDF textile fibres (Lund and Hagström 2010; Steinmann et al. 2011).

Under certain conditions, β-crystalline PVDF fibres would make it possible for each fibre to act as a piezoelectric strain sensor. To obtain a voltage from stretching, the PVDF needs to be poled, meaning that the dipolar momentums of the PVDF-molecules are aligned, which is achieved by applying a high voltage through the material. In order to do this, as well as register (harvest) the voltage output, electrodes need to be attached. For PVDF films a sandwich-structure, with conductive phases on both sides, is generally used. PVDF-fibres can also be applied in a similar sandwich-structure, but this does not make use of the full potential of the fibre format. If the conductive phases (electrodes) were instead integrated parts of the fibre in the longitudinal direction, this would offer good opportunities both for the output of piezoelectric signals and the textile flexibility (Egusa et al. 2010; Pini et al. 2007).

Conductive layers can, theoretically, be added to the fibre structure by multi-component fibre spinning. Since the piezoelectric material needs electrodes on both sides, a tri-component system, with one outer and one inner conductive phase, would be optimal. In reality, this has proven difficult to obtain, partly because it requires rare equipment, and partly because the spinning process becomes increasingly complicated to optimize with each added layer. Lund et al. (2012) produced bi-component fibres with β-phase PVDF as sheath and a conductive polymer composite (CPC) consisting of dispersed carbon black (CB) in polyethylene (PE) as core material. The fibres were inserted in a heat-pressed Co-PE/CB matrix that functioned as outer electrode. This outer electrode was mainly chosen because of its simplicity and to show that the system could be used for sensor applications, but was not refined enough to distinguish it from previously mentioned sandwich-structure, in terms of flexibility.

Egusa et al. (2010) proposed an alternate route to produce multi-component piezoelectric fibres using poly(vinylidene-flouride-triflouroethylene) copolymer (P(VDF-TrFE)) that spontaneously forms the β-phase upon solidification from the melt. They made preforms of P(VDF-TrFE) and CPC/indium electrodes that were thermally drawn into fibres of up to tens of metres of length. Although this method offers a possible route to small-scale production of piezoelectric fibres, it would not be preferred if

quantities of several kilograms were demanded. P(VDF-TrFE) is also a much more expensive material than common PVDF.

The application of the outer electrode to woven substrates of the fibres with textile coating methods would allow for industrial-scale production, if a suitable coating system was found. Common routes to conductive textile surfaces are: metallization by plating (by for example Jiang et al. 2006) or sputtering (Depla et al. 2011); in situ polymerization of intrinsically conductive polymers (ICP) (Gregory et al. 1989; Knittel and Schollmeyer 2009; Oh et al. 1999); or CPC coating (Cristian et al. 2011; Zhang et al. 2012). Metallization offers the advantage of high conductivity, but metallic surfaces are poorly adapted to the demands of a flexible sensor as cracks are easily formed by mechanical forces (Jiang and Guo 2009). In situ polymerization of ICP is difficult to perform on PVDF because of its low surface energy, especially since a high amount of ICP is necessary to obtain the required conductivity, the method has however been studied for piezoelectric ceramic fibres (Pini et al. 2007). CPC coating would be a plausible alternative, but requires optimization to maintain the drapability of the textile.

Similarly to a CPC coating, the potential of using poly(3,4-ethylene dioxythiophene)-poly(styrene sulfonate), PEDOT:PSS, as the conductive material in a textile coating formulation was investigated (Åkerfeldt et al. 2013a). The formulation consisted of a water-based polyurethane (PU) coating binder, the PEDOT:PSS dispersion, a PU-based rheology modifier and ethylene glycol (EG) as conductivity enhancer. The coatings showed good abrasion resistance when applied on a plain weave of spun polyethylene terephthalate (PET) staple fibres (Åkerfeldt et al. 2013b). Thus, depending on the coating composition, thin and flexible textile coatings were achieved with comparably low surface resistivity.

PEDOT:PSS was also studied as electrode material for piezoelectric PVDF films, both with (Lee et al. 2005; Sielmann et al. 2013) and without (Schmidt et al. 2006) the addition of a high-boiling solvent as a conductivity enhancer. Although the obtained conductivities were found to be significantly lower than for metallic coatings, the flexibility was superior and as such, the films could be stretched repeatedly without any loss of signal.

It is, admittedly, difficult to quantify the perception of a textile, but if some of it is not retained the purpose of smart textiles would inevitably be lost. Some textile testing standards relevant for the application in this study were chosen: For coated textiles, it is particularly interesting to study the change in tear strength with the coating since this is the property that is most likely to differ (Bulut and Sülar 2011). The abrasion resistance can tell something of how well the coating remains on the textile during wear, but is not demanding enough to truly challenge most coatings. Instead, shear flexing can be used, which will subject the sample both to folding and high shearing forces in a harsh manner.

So far, no papers have been found addressing the outer electrode of PVDF bicomponent fibres in a woven construction with conductive PEDOT:PSS coatings. The purpose of this study was to achieve this and to study the textile behaviour of these sensor systems in terms of tear strength, abrasion resistance and resistance to shear flexing. In contrast to previous studies of knife coating with PEDOT:PSS on textiles, the aim was here to add the conductive layer so that it enfolded individual fibres to as

great extent as possible to maximize the possible output signal from each fibre. To achieve this configuration, coatings were applied by dip coating of the substrate followed by passing through nip rollers, also known as the pad-mangle method.

Methods

Materials

Melt spun bicomponent fibres

The PVDF homopolymer was grade Kynar 705 (Arkema, France). According to the supplier, its melting point was 172°C, its melt flowindex (MFI) is 56 g/10 min at 230°C (for 2.16 kg), and its density was 1780 kg m^{-3}. The polymer used for the fibre core material was high density polyethylene (HDPE) ASPUN 6835A from Dow (Midland, MI) with a density of 950 kg/m^3, T_m = 129°C and MFI of 17 g/10 min. HDPE was compounded with 10 wt-% of carbon black (CB) of grade Ketjenblack EC-600 JD (Akzo-Nobel, Netherlands), density 1800 kg/m^3 and BET surface area of 1400 m^2/g (all data according to suppliers) in a ZSK 26 K 10.6 twin screw extruder (Coperion, Germany) as described in a previous paper (Lund et al. 2012).

Bi-component fibres were melt spun using equipment from Extrusion Systems Limited (ESL, England) equipped with two single extruders, one for the core and one for the sheath material, in this case with identical temperature settings: 190°C, 230°C and 255°C for extruder zones 1, 2, 3, respectively. The temperature of the gear pump and spinneret was set to 255°C. The spinneret had 24 holes with diameters of 0.6 mm each. A schematic description of the melt spinning equipment is seen in Figure 1. The relative rate of metering of polymer to the spinneret determined the relative amounts of core and sheath material in the fibre. Fibres were spun with a melt draw ratio (MDR = V_1/V_0) of 30 and a solid state draw ratio (SSDR = V_2/V_1) of 3. Fibre production parameters are found in Table 1. The diameter of the fibres produced was controlled by the draw ratio (MDR*SSDR) through the entire system.

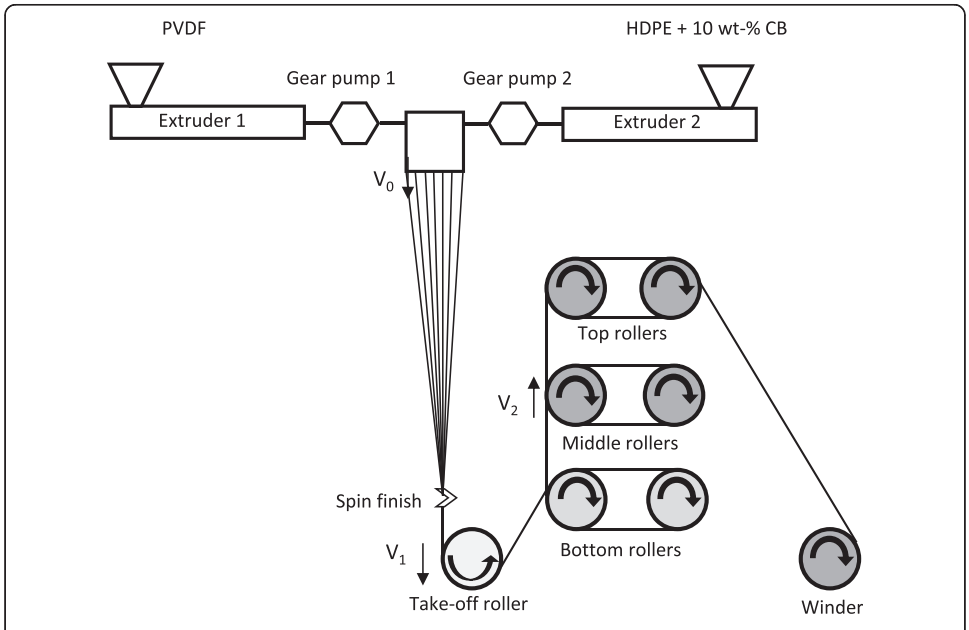

Figure 1 Schematic illustration of the melt spinning equipment.

Table 1 Fibre production parameters

MDR	SSDR	Flow rate (cm^3 min^{-1})		V_0 (m min^{-1})	V_1 (m min^{-1})	V_2 (m min^{-1})	Godet roll temp (°C)	
		Core	Sheath				Bottom	Other
30	3	7.2	28.8	5.31	155	489	90	25

The woven substrate

The multifilament fibres were woven into a plain construction with a PE monofilament warp yarn (Nm 36). The density of the woven substrate was 150 g/m^2, with 8 picks/cm in the weft and 16 ends/cm in the warp direction.

The conductive coatings

For the preparation of the outer electrode materials, two coating formulations were prepared for comparison according to Table 2: formulation A with binder and formulation B without. The conductive material was a water dispersion of PEDOT:PSS, Clevios™ PH 1000 (Heraeus Clevios GmbH, Germany) with a solids content of 1.1 wt-%, a viscosity of 33 mPa·s and an average particle diameter of 30 nm. A commercial textile coating formulation, Performax® 16297G (Lubrizol Advanced Materials Europe BVBA, Belgium), was used as the binder. The formulation was an aqueous dispersion of thermoplastic, aliphatic polyester-polyurethane with a solids content of 32 wt-%, thickened by hydroxyethyl cellulose (HEC). The rheology modifier used was an aqueous dispersion of hydrophobically modified ethoxylated urethane (HEUR) denoted Borchi® Gel L75N (Borchers GmbH, Germany), with a solids content of approximately 48 wt-%. EG (Sigma Aldrich, Germany) with a boiling point of 198°C and a viscosity of 16 mPa · s, was used as received. All data are according to suppliers.

The components of the coating formulations, see Table 2, were mixed with a stirrer (RW20, IKA®, Germany) for two minutes at 600 rpm, after which the formulations macroscopically appeared homogenous and stable.

Sample preparation

Coating

Samples sized 25 * 50 cm were prepared from the woven substrate. The coating formulations were applied to the substrate via pad-mangle (Roaches Ltd, UK). The nip pressure was 1 kPa and the speed 1.5 m/min and the resulting wet pick-up was approximately 50% for all samples. The samples were dried at 80°C for 4 minutes (labdryer LTE-S(M), Werner Mathis AG, Switzerland).

Regarding the pad-mangle coating process from a fluid-mechanical point of view, it can be viewed as a combination of dip coating and a forward two-roll coating process, see Figure 2. The dip coating is mainly governed by substrate speed, surface tension and viscosity of the formulation (with water as solvent, the effect of drying during the process is negligible); the roll coating will be influenced by the nip pressure, roll speed

Table 2 Components and solids content in weight-% of the coating formulations

Coating formulation **A**:	60% PEDOT:PSS dispersion	28% PU-binder	10% EG	2% HEUR rheology modifier	Solids content (w/o EG): 11.4%	Concentration PEDOT:PSS in coating: 6.20%
Coating formulation **B**:	80% PEDOT:PSS dispersion	0% binder	12.5% EG	7.5% HEUR rheology modifier	Solids content (w/o EG): 4.5%	Concentration PEDOT:PSS in coating: 19.6%

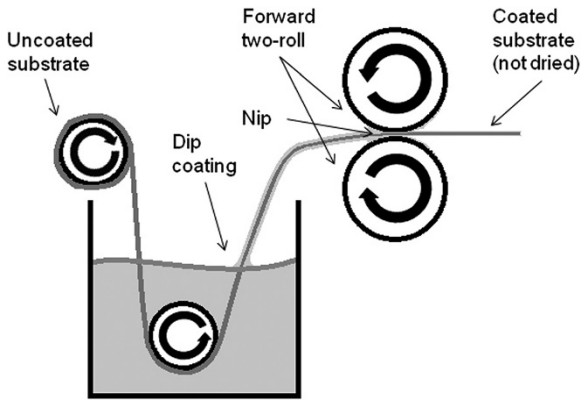

Figure 2 Schematic illustration of the pad-mangle process, indicating the dip coating and the forward two-roll coating parts.

and coating viscosity. It is difficult to determine the shear forces applicable during the entire process due to the great number of process parameters, but theoretically they have been appreciated to reach instantaneously extremely high values, of 10^3 s^{-1}. This is mainly during pulling the substrate from the bath and in the turbulent areas surrounding the nip of the rollers, in the rolling bank of the coating formulation just before the nip and in the film-splitting meniscus region, i.e. where the rollers part from each other (Kistler and Schweizer 1997).

PVDF is generally known to have a very low surface energy due to the flourine incorporated to its structure. Therefore, hydro- and even oleophobicity are inherent properties of PVDF and as a consequence, the adhesion to other materials can be a difficulty. The formulations were thickened to a higher viscosity than what is commonly suggested for pad mangle coating; the purpose of this being to obtain as much pick-up of the coating on the substrate as possible, thus resulting in better contacting of the PVDF. With the subsequent passing through nip rollers, the excess coating was squeezed out, but enough coating formulation was constrained to obtain a macroscopically coherent coating after drying.

Poling

The woven substrate was cut into strips in the weft (PVDF-bicomponent yarn) direction. The conductive cores of the yarns were contacted with a CB-PE matrix, heat-pressed onto the end of each strip. The cores were connected to ground and the strip put into a construction with needles pointing towards the fibre surfaces. The specimen, with the needle construction, was put into an oven at 75°C. A voltage of −10 kV was applied through the needles during 5 minutes before both heat and voltage were turned off and the sample was allowed to cool to room temperature before removal from the oven. This procedure was shown to be sufficient to orient the dipoles by Nilsson et al. 2013.

Characterization

FT-IR

The crystallinity in the fibres was evaluated with attenuated total internal reflectance Fourier transform infrared spectroscopy (ATR-FTIR), using Bruker Tensor 27 and software Opus 7.2 (Bruker Optik GmbH, Germany).

Piezoelectric characterization

The coated strips were subjected to dynamic strain using a servo-hydraulic tensile testing machine (Model 66-21B-01, MTS systems, USA). Each sample was clamped between two rubber sheets, to prevent sliding and for electrical isolation. The starting distance between the clamps was set on 100 mm. After the sample was secured between the clamps a pre-tension force of 15.4 N was applied in order to prevent slack in the sample during measurement.

All samples were exposed to a sinusoidal strain with amplitude of 1%. The sensor electrodes were connected to a data acquisition device (with an input impedance of 100 GΩ in parallel with 100 pF) (NI DAQPad-6016, National Instruments, USA) connected to a computer running a LabVIEW Software, which controlled the measurement. The piezoelectric output voltage from the fibres was recorded at 3 Hz, which gives the intrinsic piezoelectric voltage. In addition, an analog signal from the MTS machine proportional to the strain was recorded.

Surface resistivity

Surface resistivity measurements were performed using a multimeter (Fluke 8846A, USA) in a four-wire resistance mode and an in-house designed and produced four-point probe, details published elsewhere (Åkerfeldt et al. 2013b). A weight of 2.2 kg was placed on the probe, and the resistivity values were read after one minute according to standard CEI/IEC 93:1980.

Scanning electron microscopy (SEM)

The appearance of the samples was studied using field emission scanning electron microscopy (FE-SEM) (JEOL JSM-7800 F, Japan). The SEM was equipped with energy dispersive spectroscopy (EDS) (Quantax X-ray mapping system, Bruker Nano GmbH, Germany), allowing elemental analysis of the samples. The samples with destroyed conductive coatings due to the flexing treatment were sputtered with a layer of 2 nm platinum. Cross-sections of the samples were embedded in epoxy, frozen to - 60°C and polished with a broad ion beam (BIB). The specimens were also sputtered with carbon by means of resistance vaporization to a thickness of 5 nm. The cross-sections were imaged with a back scatter detector and EDS-mapping.

Stress viscometry

The shear viscosity of the coating formulations was evaluated with a stress-controlled rheometer (Bohlin CS Melt, Sweden) and a cone-and-plate set-up. Samples were subjected to stress sweeps, for coating A 1.62-55.5 Pa and for coating B 0.31-367 Pa, corresponding to a similar range of shear rates for the two samples, of approximately 0.015-180 s^{-1}.

Tear strength

Tear strength in the warp direction (the bi-component weft yarns torn) was determined according to standard EN ISO 4674-1B in a tensile tester (Instron 4502, UK). A minimum of three replicas of each sample was tested.

Abrasion resistance

Abrasion was studied using a Martindale (Nu-Martindale model 403, James Heal & Co. Ltd, UK) and wool abradant fabric, according to standard EN ISO 5470–2. The sample

holders were in accordance with standard EN ISO 12945–2 (diameter 90 mm). The effect of the abrasion was evaluated based on resistivity measurements and surface appearance as described above. The total weight on each sample during abrasion was 563 g. Three replicas of each sample were abraded, and the mean values with standard deviations calculated.

Resistance to shear flexing

Testing for resistance to shear flexing was performed in accordance with ISO standard 5981:2007 (method B, without pressure foot) in an apparatus specifically constructed for this test method (Meadowbank Innovations Ltd, UK). Samples were in the size of 100 mm in the weft direction and 50 mm in the warp direction, allowing them to be clamped into the adjacent holders and leaving an area of 2250 mm^2 of fabric between that was folded and subsequently subjected to shearing when the holders moved juxtaposed each other. The samples were subjected to 1000 cycles each, where after their surface resistivity was measured in accordance with previous description.

Results and discussion

The piezoelectric effect

The piezoelectric characterization showed that both coatings performed the function of outer electrodes to the fibres. The voltage output was above 12 V peak-to-peak at a frequency of 3 Hz and with a strain of 1%, as depicted with the diagrams for the coatings in Figure 3. Previous, unpublished work using this method showed a large variation in data, in spite of the clear and high output signal from the measurements. This means that no difference in response between the coatings could be ascertained with this method, but it is plausible that a more rigorous measurement set-up would be able to better grade the samples with respect to piezoelectricity.

Figure 4 illustrates schematically how the piezoelectric tri-component system works on an individual fibre level. The dipoles are expected to be oriented radially outwards from the nucleus towards the shell, so stretching the fibre as in Figure 4a means that the dipoles are uniformly compressed, resulting in a piezoelectric effect, detected as the voltage output (Nilsson et al. 2013). The tri-component electrode configuration in

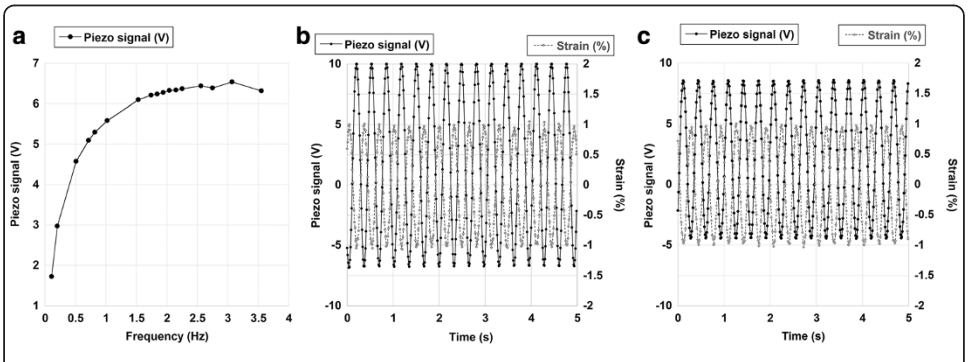

Figure 3 a) Piezo signal (voltage output) from a representative sample (in this case coating B) versus the frequency of the strain, b) piezo signal (voltage output) of a sample with coating A versus strain and over time, c) piezo signal (voltage output) of a sample with coating B versus strain and over time.

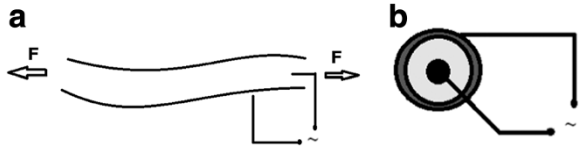

Figure 4 Schematic illustration of the stretching and concurrent contraction in the cross-section of the PVDF fibre, a) from side-view, b) of a cross-section of one single fibre (the brighter area signifies the PVDF) with a conductive core and shell (darker areas) as electrodes for the voltage signal.

Figure 4b, with the outer electrode enfolding the fibre entirely, is believed to result in the maximum voltage output from the system because it maximizes the contact areas to the piezoelectric PVDF. Although this idealized structure is complicated to achieve continuously by employing only the fibre spinning process, the results here show that, in terms of yielding the piezoelectric effect, sufficiently similar structures were achieved with conductive coatings on bi-component fibres.

Since the piezoelectricity of PVDF depends on the presence of β-phase crystallinity in the polymer, the β-phase was verified with FT-IR and a representative spectrum of the PVDF fibres is included in Figure 5. The vibrational band at 840 cm^{-1} is indicative for β- or γ-phase crystallinity in PVDF; it is here related to the β-phase since the crystallinity in these fibres was formed during the solid state drawing process (≤80°C) and γ-phase is only formed by crystallization at temperatures close to T_m of the α-phase (≥166°C) (Gregorio 2006; Guo et al. 2013). The bands at 764, 855 and 976 cm^{-1} are typical of the α-phase, and no distinct peaks can be seen in these regions in Figure 5, indicating a very low content of α-phase crystallinity.

The coated textiles

Two coating formulations were compared for the application, see Experimentals and Table 2. The purpose was to evaluate whether the binder had a relevant function for

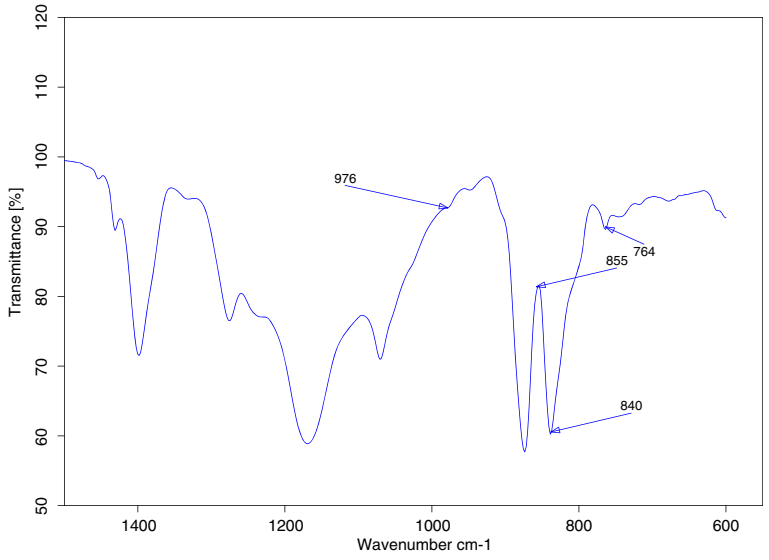

Figure 5 FT-IR spectrum for the PVDF fibres.

the coating, since it was known that the binder molecules could hinder the conductivity of the PEDOT:PSS. Macroscopically, the coated textiles appeared similar with regard to handle and aesthetic properties.

Surface resistivity

The surface resistivity measurements showed a difference of about one order of magnitude between the coatings, see Table 3, where the increased contents of PEDOT:PSS and EG in coating B favoured lower resistivity. The resistivity of coating A was found to average at 134 Ω/square, whereas coating B averaged at 12.3 Ω/square. As concluded from the piezoelectric test, in spite of this rather significant difference, the conductivity of both coatings was sufficient for the application as outer electrodes. Although it is reasonable to assume that electrodes with higher conductivity should yield a stronger signal in the piezoelectric response, it is not the only significant property for the application. The distribution of the coating on the individual fibres and its durability during use would also be critical factors.

Distribution of the conductive coatings

To evaluate the distribution of the coatings in the PVDF fibre bundles, the sulphur of the PEDOT:PSS and the fluorine in the PVDF fibres were used for mapping with EDS. EDS-mapping was initially performed on dried films of the coating with and without PEDOT:PSS, see Figure 6. The spectra showed no indication of sulphur in the coating without PEDOT:PSS and a small, but distinctive, sulphur peak for the coating with PEDOT:PSS.

The EDS-images in Figure 7 show the sulphur mapping of the cross-sections of the samples, where the sulphur signal is represented with the brighter areas. From the dark noise that constitutes the rest of the images it is possible to distinguish the bi-component fibres with their darker cores and also a darker area in the upper part of the image in Figure 7b, which is the PE monofilament warp. Both images depict the same orientation of the fibre bundles in relation to the warp, so the penetration of the coatings occurred from below and went upwards. Sulphur is the element that discerns the conductive material from the other organic molecules and although the low atomic content of sulphur was a challenge in the mapping, the EDS-images in Figure 7 thus provide a skeletal structure of the conductive pathways in the coatings. The images showed that both coatings have penetrated quite well into the woven substrate, reaching beneath the fibre bundles of the weft towards the warp intersections. Coating A appears as though it penetrated too well, and coating B appears better distributed in the weft fibre bundles themselves, closer to the idealized tri-component structure.

The PU-binder formulation present in coating A is strongly pseudoplastic due to its thickener HEC, whereas coating B is only thickened with a HEUR rheology modifier, see Table 2. Also, formulation B has a solids content of almost only a third of that of

Table 3 Surface resistivity of samples coated with formulation A and B

Sample	Coating A	Coating B
Initial surface resistivity (Ω/square)	134	12.3
Surface resistivity after Martindale (50 000 cycles) (Ω/square)	171	74
Surface resistivity after shear flexing (1000 cycles) (Ω/square)	10 700	535 000

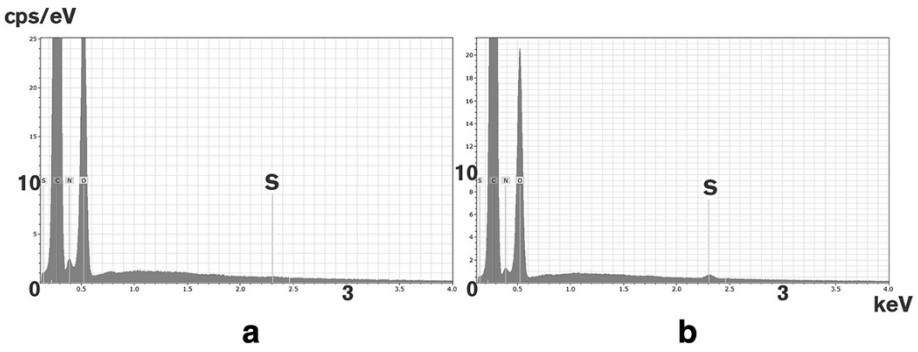

Figure 6 EDS-spectra of films made of a) the coating without PEDOT:PSS, and b) the coating with PEDOT:PSS.

formulation A. From the shear viscometry presented in Figure 8, coating B has a significantly more Newtonian behaviour with a more steady viscosity both during the high shear forces of the coating procedure as well as during the low shear of the drying process than coating A. Coating A appears more influenced by the binder formulation and its thickener than the HEUR and could be expected to flow very well during extremely high shear, but will soon return to its high viscosity state when these forces cease (Ascanio and Ruiz 2006; Davard and Dupuis 2002; Glass and Prud'homme 1997). This could explain the distributions of the coatings from the images in Figure 7, where coating A penetrated more below the fibre bundle than coating B.

Microstructure

The microstructure of the coatings on the PVDF fibres was also studied with SEM and EDS. Figure 9 contains the representative SEM-images of the coated weft insertions and the subsequent sulphur mapping with EDS, with coating A in Figure 9a-b and coating B in Figure 9c-d. The images show the PVDF bi-component fibre bundles framed by the much larger (in fibre diameter) PE monofilaments; the initial SEM in this figure did not reveal any distinct differences between the coatings, coating A is difficult to detect as it is more of a blurry feature on the fibres and coating B is mainly detected closer to the warp intersections where it seems to have accumulated. Regarding the images with sulphur mapping to the right, where the sulphur is represented as the brighter features, differences become increasingly clear. Coating A had a dappled appearance in the EDS-images, illustrated in Figure 9b, probably deriving from phase separation of the different

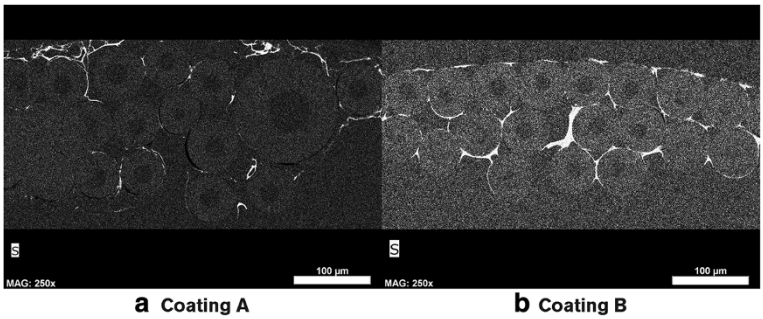

Figure 7 EDS sulphur mapping of the cross-sections: a) with coating A and b) with coating B.

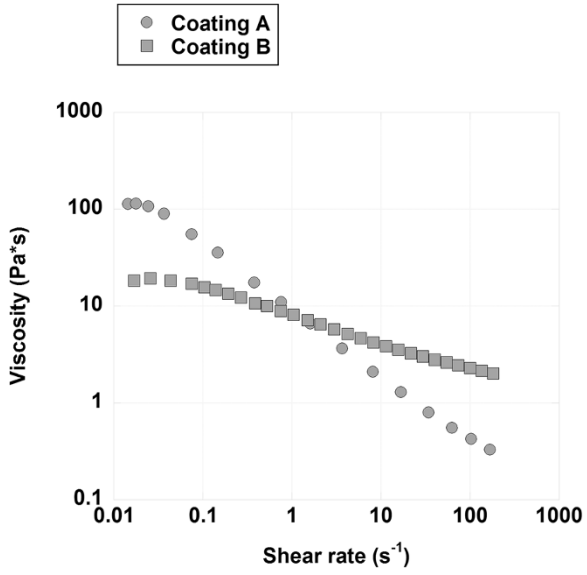

Figure 8 Steady state shear viscometry of the coating formulations.

polymers. Coating B, in Figure 9d, showed a much more even appearance, except for where the fibres strike through in the image. Mapping of the fluorine in these images (not shown) further showed that for coating A there were areas neither rich in sulphur nor fluorine, but rich in carbon; indicating areas of the coated textiles that were neither void, PEDOT:PSS or PVDF, but rather the PU-binder. The corresponding mapping of coating B showed a visible signal from either sulphur or fluorine throughout the image.

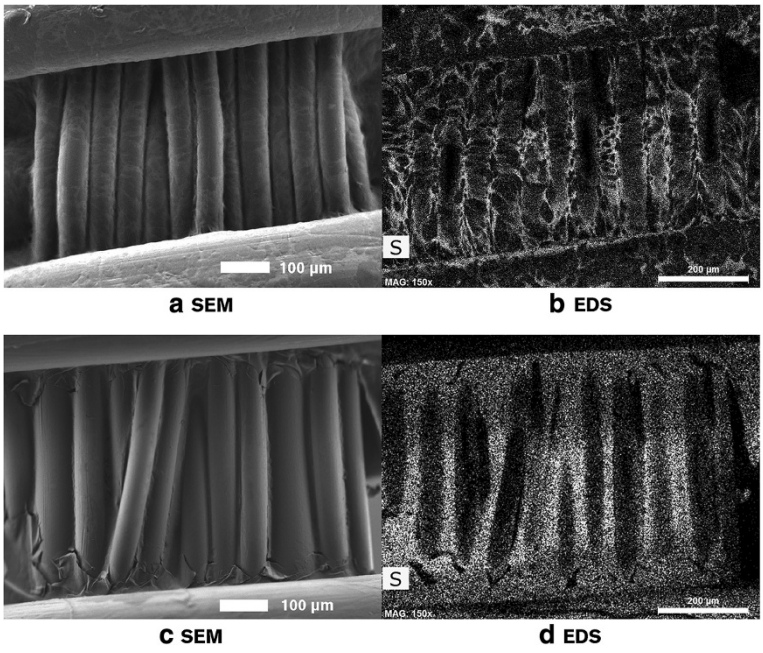

Figure 9 SEM-images and sulphur mapping (EDS) of the coated weft insertion of the samples, top-view: a-b) with coating A and c-d) with coating B.

Surface sensitive imaging was performed with low voltage SEM, illustrated in Figure 10a-b for coating A and 10c-d for coating B, in order to better distinguish the coatings from the textile substrate. EDS-mapping showed that the brighter areas in these images contained sulphur, indicating the PEDOT:PSS, the darkest areas contained fluorine, indicating the PVDF fibre, and the medium grey areas, visible at the higher magnification in Figure 10a, were of organic material, indicating the polyurethane. The distribution of the polyurethane in the PEDOT:PSS is seen in the higher magnification (2000x) in Figure 10b, showing a feather-like pattern of polyurethane bridging between the fibres and the PEDOT:PSS. Coating B, in Figure 10c, was distinctly different in character from coating A as no phase separation was indicated; it appeared as a smooth and rather homogenous film was formed on the substrate. Several cracks were visible close to the warp intersections, indicating a lack of flexibility in this coating. At a higher magnification (2000x), Figure 10d, the film has a grooved structure and appears to be very thin and frail. These observations corroborate those made in relation to Figure 9 and clarify the differences between the coatings.

It is relevant to compare the top view mapping of the samples in Figures 9 and 10 with the distribution of the coatings showed in Figure 7. The top-view images showed coating on the top of the weft yarn for both coatings, so even coating A enfolded the weft yarns, though probably to a lesser extent than coating B. Due to the phase separation of coating A, the distribution of the PEDOT:PSS was however less homogeneous than in coating B. Considering the surface resistivity, it can be concluded that the relatively small amounts of the coatings and their distribution was still sufficient to form a reasonably conductive network.

To understand how the microstructure of the coatings affected the conductivity in greater detail, it is required to look at the approximated compositions of the dried

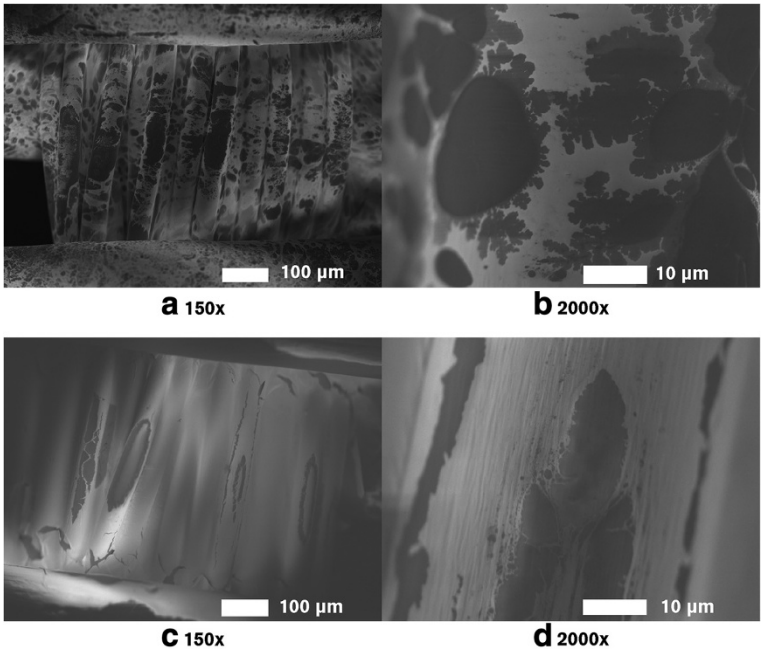

Figure 10 Low voltage (100 V) SEM- images of the coated weft insertion of the samples: a-b) with coating A and c-d) with coating B.

coatings. The PEDOT:PSS concentration in the dried coatings was about 6 wt-% for coating A and 20 wt-% for coating B, not taking the liquid EG into account (see Table 2). Also, in coating A, up to 90 wt-% of the solids content is the high molecular weight polyurethane, whereas in coating B the only other solid is the HEUR, which is of more oligomeric size. The morphologies depicted in the low voltage SEM-images in Figure 10 shows that PEDOT:PSS and HEUR seem to blend with each other a lot better than PEDOT:PSS and PU, which may be a result of the more compatible sizes of the molecules. However, with the lower amount of solids in coating B and since both coatings were picked up by the substrate to the same extent, the actual amount of PEDOT:PSS per square meter (A: 0.53 g/m^2 and B: 0.66 g/m^2) is about the same for both coatings. Comparing with the initial resistivities of the coatings in Table 3, it appears as though the PU-binder in coating A does hinder the conductivity of the PEDOT:PSS clusters, with one order of magnitude.

Textile properties and durability

The tear strength of the uncoated substrate was 242 N, as depicted in Figure 11; it decreased almost 30% with formulation A, and increased by more than 30% with formulation B. This is in agreement with previous results (Åkerfeldt et al. 2013b) where it was concluded that increased amounts of binder polymers increased the brittleness of a PET substrate, making the yarns more brittle, whereas increased PEDOT:PSS and EG amounts led to increased ductility, with respect to tear strength and bending rigidity. The tear strength of textiles is generally deteriorated after coating because the coating glues the fibres together in bundles and reduces the mobility of the fibres/yarns vis-à-vis each other (Bulut and Sülar 2011). It is however highly interesting that coating B instead increased the tear strength of the samples and a possible explanation could be a plasticizing effect of coating B, i.e. that the inter-fibre friction decreased.

The tear strength is indicative of how the coating and the textile interact and as such a good tool to evaluate coated textiles, whereas the durability tests tell more about the

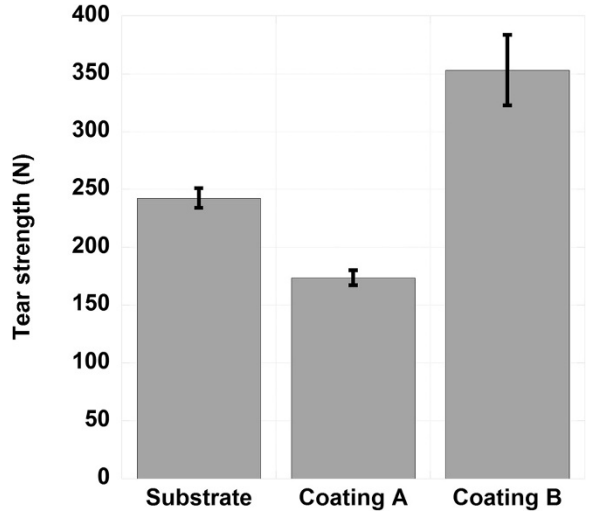

Figure 11 The mean values of triplets of the tear strength measurements of the samples, with standard deviations represented.

coating, especially how well it adheres to the textile fibres (Sen 2008). From Table 3, the initial surface resistivity measurements of the coated textiles show a difference of about one order of magnitude, where coating B has the lower resistivity. After 50 000 abrasion cycles, the resistivity of the samples with coating B increased with five times (500%) of its original value, whereas the samples coated with A only increased with 28% of its original value. After the flexing test, also in Table 3, the coating without binder (coating B) has lost almost all of its conductivity while the coating with the binder (coating A) has maintained a reasonable conductivity, with an increase of two orders of magnitude in resistivity.

The SEM-images in Figure 12a-d show the influence of the flexing treatment on the coatings, at different magnifications and by tilting the samples. Comparing with the previous SEM-images of the initial coatings in Figures 9 and 10 there is indication of considerable distortion on the coatings, especially on coating B: coating A appears as smeared and stringy, but still allows some conductive networking; coating B on the other hand has cracked and seems to have disjoined from the substrate, leaving the conductive network entirely broken. This is especially apparent at the 350 times magnification of the warp and weft intersections; coating B has sharp, broken edging and coating A remains somewhat intact. These images are in good agreement with the previously discussed resistivity measurements (see Table 3). Correlating this result with that in relation to the high magnification image of the phase separation in Figure 10b, it is indicated that it is a bridging of the binder between the PEDOT:PSS and the PVDF fibres that holds the system together and avoids the disunion. It is also worth mentioning that the lost conductivity after the flexing of the samples with coating B, i.e. without the bridging binder, also gave rise to charging in the SEM, even at very low accelerating

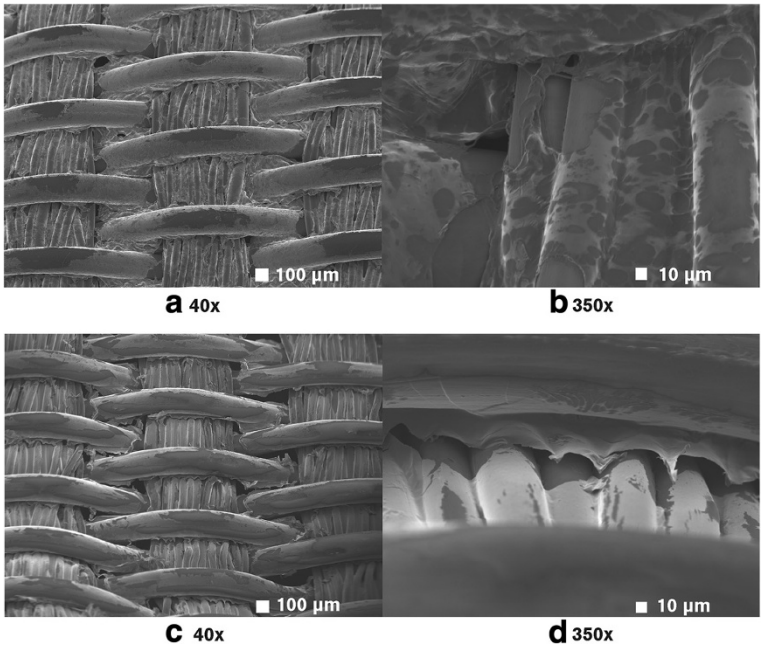

Figure 12 SEM-images of samples subjected to 1000 cycles of shear flexing: a-b) with coating A and c-d) with coating B.

voltages, and sputtering with platinum was necessary in order to achieve comparable images of the two coatings.

Conclusions

Coatings of PEDOT:PSS were successfully used as outer electrode material for a woven substrate of bi-component PVDF fibres, with the potential application of a piezoelectric strain sensor. The coatings were thin, macroscopically flexible and exhibited a surface resistivity in between 10–150 Ω/square. The coated textiles without binder exhibited an initially lower resistivity than those with the binder, but did not withstand flexing to the same extent. SEM showed that the coating without binder flaked off and the resistivity increased drastically after 1000 cycles whereas the coating with the binder was rubbed off with less increase in resistivity. Both coatings had reasonable tear strength, but the inclusion of binder polymers was necessary for their durability. A tougher system, but with retained conductivity, would be desired and other types of binder polymers will therefore be the subject of future study.

Competing interests
The authors declare that they have no competing interests.

Authors' contributions
MÅ carried out the experimental work on the textiles and drafted the manuscript, EN made the fibresand wrote the experimental parts regarding these, PG and PW were active in the planning and participated in the sequence alignment of the paper. All authors read and approved the final manuscript.

Acknowledgements
The authors thank Lars Eklund (Swerea IVF) and Professor Bengt Hagström (Swerea IVF) for their invaluable scientific guidance during the course of this work. Financial support is gratefully acknowledged to Swedish Foundation for Strategic Research (SSF), Sparbanksstiftelsen Sjuhärad and, through the Smart Textiles initiative, VINNOVA.

Author details
[1]Swerea IVFAB, Textiles and Plastics Department, Box 104, SE-43122 Mölndal, Sweden. [2]University of Borås, The Swedish School of Textiles, SE-50190 Borås, Sweden. [3]Chalmers University of Technology, Materials and Manufacturing Technology, SE-41296 Gothenburg, Sweden.

Received: 8 April 2014 Accepted: 20 August 2014
Published online: 25 September 2014

References

Åkerfeldt, M, Stråat, M, & Walkenström, P. (2013a). Electrically conductive textile coating with a PEDOT-PSS dispersion and a polyurethane binder. *Textile Research Journal, 83*(6), 618–627. doi:10.1177/0040517512444330.

Åkerfeldt, M, Stråat, M, & Walkenström, P. (2013b). Influence of coating parameters on textile and electrical properties of a poly(3,4-ethylene dioxythiophene):poly(styrene sulfonate)/polyurethane-coated textile. *Textile Research Journal, 83*(20), 2164–2176. doi:10.1177/0040517513487786.

Ascanio, G, & Ruiz, G. (2006). Measurement of pressure distribution in a deformable nip of counter-rotating rolls. *Measurement Science and Technology, 17*(9), 2430.

Bulut, Y, & Sülar, V. (2011). Effects of process parameters on mechanical properties of coated fabrics. *International Journal of Clothing Science and Technology, 23*(4), 205–221. doi:10.1108/09556221111136476.

Cristian, I, Nauman, S, Cochrane, C, & Koncar, V (Eds.). (2011). *Electro-conductive sensors and heating elements based on conductive polymer composites in woven structures*. Rijeka, Croatia: InTech.

Davard, F, & Dupuis, D. (2002). Blade coating of fabrics: rheology and fluid penetration. *Coloration Technology, 118*(2), 69–74. doi:10.1111/j.1478-4408.2002.tb00140.x.

Depla, D, Segers, S, Leroy, W, Van Hove, T, & Van Parys, M. (2011). Smart textiles: an explorative study of the use of magnetron sputter deposition. *Textile Research Journal, 81*(17), 1808–1817. doi:10.1177/0040517511411966.

Egusa, S, Wang, Z, Chocat, N, Ruff, ZM, Stolyarov, AM, Shemuly, D, & Fink, Y. (2010). Multimaterial piezoelectric fibres. [Letter]. *Nature Materials, 9*(8), 643–648. doi:10.1038/nmat2792.

Fukada, E, & Takashita, S. (1969). Piezoelectric effect of polarized poly (vinylidene Flouride). [Short note]. *Japan Journal of Applied Physiology, 8*, 960.

Glass, JE, & Prud'homme, R. (1997). Coating rheology: component influence on the rheological response and performance of water-borne coatings in roll applications. In S Kistler & P Schweizer (Eds.), *Liquid film coating* (pp. 137–182). Dordrecht, Netherlands: Springer Netherlands.

Gregorio, R. (2006). Determination of the α, β, and γ crystalline phases of poly(vinylidene fluoride) films prepared at different conditions. *Journal of Applied Polymer Science, 100*(4), 3272–3279. doi:10.1002/app.23137.

Gregory, RV, Kimbrell, WC, & Kuhn, HH. (1989). Conductive textiles. *Synthetic Metals, 28*(1–2), 823–835.

Guo, Z, Nilsson, E, Rigdahl, M, & Hagström, B. (2013). Melt spinning of PVDF fibers with enhanced β phase structure. *Journal of Applied Polymer Science, 130*(4), 2603–2609. doi:10.1002/app.39484.

Jiang, SQ, & Guo, RH. (2009). Modification of textile surfaces using electroless deposition. In Q Wei (Ed.), *Surface modification of textiles* (pp. 108–125). Cambridge: Woodhead Publishing Ltd. Retrieved from http://dx.doi.org/10.1533/9781845696689.108.

Jiang, SQ, Newton, E, Yuen, CWM, & Kan, CW. (2006). Chemical silver plating on cotton and polyester fabrics and its application on fabric design. *Textile Research Journal, 76*(1), 57–65. doi:10.1177/0040517506053827.

Kawai, H. (1969). The piezoelectricity of poly (vinylidene Flouride). [Short note]. *Japan Journal of Applied Physiology, 8*, 975–976.

Kirstein, T. (2013). The future of smart-textiles development: new enabling technologies, commercialization and market trends. In T Kirstein (Ed.), *Multidisciplinary know-how for smart-textiles developers* (pp. 1–26). Woodhead Publishing Ltd. Retrieved from http://dx.doi.org/10.1533/9780857093530.1.

Kistler, SF, & Schweizer, PM. (1997). *Liquid film coating: scientific principles and their technological implications (SpringerLink, Archive ed.)*. Dordrecht: Springer Netherlands.

Knittel, D, & Schollmeyer, E. (2009). Electrically high-conductive textiles. *Synthetic Metals, 159*(14), 1433–1437.

Lee, SH, & Cho, HH. (2010). Crystal structure and thermal properties of poly(vinylidene fluoride)-carbon fiber composite films with various drawing temperatures and speeds. *Fibers and Polymers, 11*(8), 1146–1151. doi:10.1007/s12221-010-1146-x.

Lee, CS, Joo, J, Han, S, & Koh, SK. (2005). An approach to durable PVDF cantilevers with highly conducting PEDOT/PSS (DMSO) electrodes. *Sensors and Actuators A: Physical, 121*(2), 373–381. doi:http://dx.doi.org/10.1016/j.sna.2005.03.005.

Lund, A, & Hagström, B. (2010). Melt spinning of poly(vinylidene fluoride) fibers and the influence of spinning parameters on β-phase crystallinity. *Journal of Applied Polymer Science, 116*(5), 2685–2693. doi:10.1002/app.31789.

Lund, A, Jonasson, C, Johansson, C, Haagensen, D, & Hagström, B. (2012). Piezoelectric polymeric bicomponent fibers produced by melt spinning. *Journal of Applied Polymer Science, 126*(2), 490–500. doi:10.1002/app.36760.

Nilsson, E, Lund, A, Jonasson, C, Johansson, C, & Hagström, B. (2013). Poling and characterization of piezoelectric polymer fibers for use in textile sensors. *Sensors and Actuators A: Physical, 201*(0), 477–486. doi:http://dx.doi.org/10.1016/j.sna.2013.08.011.

Oh, KW, Hong, KH, & Kim, SH. (1999). Electrically conductive textiles by in situ polymerization of aniline. *Journal of Applied Polymer Science, 74*(8), 2094–2101. doi:10.1002/(sici)1097-4628(19991121)74:8<2094::aid-app26>3.0.co;2-9.

Pini, N, Busato, S, Elsener, H-R, & Ermanni, P. (2007). In situ growth of interdigitated electrodes made of polypyrrole for active fiber composites. *Polymers for Advanced Technologies, 18*(3), 249–253. doi:10.1002/pat.883.

Schmidt, VH, Lediaev, L, Polasik, J, & Hallenberg, J. (2006). Piezoelectric actuators employing PVDF coated with flexible PEDOT-PSS polymer electrodes. *Dielectrics and Electrical Insulation, IEEE Transactions on, 13*(5), 1140–1148. doi:10.1109/tdei.2006.247842.

Schwarz, A, Van Langenhove, L, Guermonprez, P, & Deguillemont, D. (2010). A roadmap on smart textiles. [Article]. *Textile Progress, 42*(2), 99–180. doi:10.1080/00405160903465220.

Sen, AK. (2008). *Coated textiles: principles and applications* (2nd ed.). Boca Raton: CRC Press.

Sielmann, CJ, Busch, JR, Stoeber, B, & Walus, K. (2013). Inkjet printed all-polymer flexural plate wave sensors. *IEEE Sensors Journal, 13*(10), 4005–4013. doi:10.1109/jsen.2013.2264930.

Steinmann, W, Walter, S, Seide, G, Gries, T, Roth, G, & Schubnell, M. (2011). Structure, properties, and phase transitions of melt-spun poly(vinylidene fluoride) fibers. *Journal of Applied Polymer Science, 120*(1), 21–35. doi:10.1002/app.33087.

Zhang, R, Deng, H, Valenca, R, Jin, J, Fu, Q, Bilotti, E, & Peijs, T. (2012). Carbon nanotube polymer coatings for textile yarns with good strain sensing capability. *Sensors and Actuators A: Physical, 179*(0), 83–91. doi:10.1016/j.sna.2012.03.029.

doi:10.1186/s40691-014-0013-6
Cite this article as: Åkerfeldt *et al.*: **Textile piezoelectric sensors – melt spun bi-component poly(vinylidene fluoride) fibres with conductive cores and poly(3,4-ethylene dioxythiophene)-poly(styrene sulfonate) coating as the outer electrode.** *Fashion and Textiles* 2014 **1**:13.

Submit your manuscript to a SpringerOpen journal and benefit from:

► Convenient online submission
► Rigorous peer review
► Immediate publication on acceptance
► Open access: articles freely available online
► High visibility within the field
► Retaining the copyright to your article

Submit your next manuscript at ► springeropen.com